Applied Catalysis B: Environmental 126 (2012) 47–54

Contents lists available at SciVerse ScienceDirect

Applied Catalysis B: Environmental

journal homepage: www.elsevier.com/locate/apcatb

Improved visible light photocatalytic activity of TiO_2 co-doped with Vanadium and Nitrogen

R. Jaiswal [a], N. Patel [b,*], D.C. Kothari [a], A. Miotello [b]

[a] Department of Physics and Centre for Nanosciences & Nanotechnology, University of Mumbai, Vidyanagari, Santacruz (E), Mumbai 400098, India
[b] Dipartimento di Fisica, Università degli Studi di Trento, I-38123 Povo (Trento), Italy

ARTICLE INFO

Article history:
Received 4 April 2012
Received in revised form 6 June 2012
Accepted 12 June 2012
Available online 8 July 2012

Keywords:
Photocatalytic degradation
Rhodamine B
Codoping TiO_2
Sol–gel method
Ball milling

ABSTRACT

V- and N-codoped TiO_2 photo-catalyst is synthesized by sol–gel method to sensitize TiO_2 to visible light. The concentrations of V and N were varied and optimized to enhance photo-catalytic activity. In order to increase the active surface area, the crystalline powder was ball milled to obtain nanosized particles. The photo-catalysts were characterized by Micro-Raman, TEM, XPS and UV–vis (in diffused reflectance mode) techniques. The co-doped TiO_2 photocatalyst displayed narrower band gap (2.3 eV) compared to singly doped TiO_2 catalyst, namely V (2 at.%)-doped (2.42 eV), N (4 at.%)-doped (2.95 eV), and undoped TiO_2 (3.13 eV). The photocatalytic activity for the degradation of Rhodamine B (an organic dye) under visible light irradiation obtained with co-doped TiO_2 photo-catalyst is significantly better as compared to the undoped, V-doped, and N-doped TiO_2. The incorporation of V and N in TiO_2 lattice induces isolated energy levels near the conduction and valence bands, respectively, causing an effective narrowing of the band gap. In addition, due to the low dopants concentrations, these energy levels can also act as traps for photoexcited holes or electrons thus reducing the recombination between photo-generated charges. Both these effects, namely band narrowing and enhanced charge separation produce synergistic effects to increase the photocatalytic activity of V-N-codoped TiO_2.

1. Introduction

The textile industries dump large amount of polluted water, especially dye solutions, in the environment. These textile dyes constitute one of the largest groups of organic compounds that are toxic to microorganism, aquatic life and human beings, and constituting a serious concern to the ecosystem [1]. Several techniques such as absorption on carbon, ultrafiltration, reverse osmosis, coagulation by chemicals, etc., have been used in the past to remove the dye pollutants [2,3]. However, these methods produce secondary pollutants which require further treatment, thus increasing the cost of the process. Photocatalysis is one of the best routes for the degradation of dyes to harmless products (H_2O and CO_2) in waste water [4].

TiO_2 is the most extensively studied semiconductor for the photocatalytic applications mainly due to its high corrosion and photocorrosion resistance in aqueous media, energy band edges which are well-matched with the redox potential of water, electronic properties that can be varied by just changing the lattice defect chemistry or the oxygen stoichiometry, environmental friendliness, easy availability and cost effectiveness [5]. However TiO_2, having an energy band gap of about 3.2 eV, mostly absorbs the ultraviolet portion of the solar spectrum and only a small amount of visible light [6]. Thus, for efficient photocatalytic activity it is necessary to extend the photo-response of TiO_2 to the visible spectrum by modification of its structure/composition. Another problem is the high recombination rate of photo-generated electron–hole pairs. The recombination can be limited by introducing charge traps for electrons and/or holes, thus increasing their lifetimes [7]. Many methods have been proposed to solve these problems, but doping TiO_2 with foreign ions is one of the most promising strategies, both for sensitizing TiO_2 to visible light and creating distinct charge traps for electrons and holes so that they remain separated [6].

TiO_2 doped with transition metals such as Cr, Fe, V, Mn, and Cu have been used in the past to improve the visible light absorption [8–10]. However, these dopant metals have to be used in small quantity to avoid recombination of photogenerated electrons and holes, which is bolstered by the large amount of these dopant species [11]. But the low content of metal doping leads to only small shift in the absorption edge of TiO_2 towards visible region. Generally, metals dopant such as V, Cr, and Mn form energy levels below the conduction band edge [12,13]. Doping TiO_2 with non-metallic anion such as N, S, and C replaces O in the TiO_2 lattice to generate energy levels just above the top of the valence band of TiO_2 to effectively narrow the band gap [14,15]. Thus, a low concentration codoping of cations and anions should be able to both enhance the

* Corresponding author.
E-mail address: patel@science.unit.it (N. Patel).

0926-3373/$ – see front matter © 2012 Elsevier B.V. All rights reserved.
http://dx.doi.org/10.1016/j.apcatb.2012.06.030

visible light absorption efficiency and reduce the recombination of the photogenerated charges. Among the transition metals, V doping TiO_2 in low concentration has shown enhanced photocatalytic efficiency both because of the increased lifetime of photogenerated charges and the extension of the absorption range [16]. Klosek and Raftery synthesized V-doped TiO_2 photocatalysts which were quite active in the visible range (396–450 nm) when used for the oxidation of ethanol [17]. N is well known anion dopant which can replace oxygen in the TiO_2 lattice and has been used in the past to decompose organic compounds [18]. Asahi et al. carried out first-principle calculations and demonstrated that N-doped TiO_2 could enhance the photoactivity under visible irradiation, owing to band-gap narrowing [19]. However, only few reports are published on V- and N-codoped TiO_2 [20,21]. Liu et al. [20] and Gu et al. [21] codoped TiO_2 with V and N to enhance the degradation of methyl blue dye and of pentachlorophenol, respectively, as compared to the single element doped TiO_2. However, in present study the concentrations of V and N are optimized in order to obtain better visible light absorption with minimum recombination problems for the degradation of organic dye. In a recent review article, Zhang et al. [22] showed that N-TiO_2 modified with metal ions, or metal oxides, or nonmetals, usually exhibit more favorable visible-light absorption and photocatalytic activity as compared to N-doped TiO_2. The synergistic effects created by the combination of the two dopants were responsible for the good photocatalytic performance.

In the present work, V- and N-codoped TiO_2 photocatalyst powder was synthesized by sol–gel method. This V-N codoped TiO_2 was compared to V-doped and N-doped TiO_2 for photocatalytic degradation of Rhodamine B (RhB) dye solution. The enhanced photocatalytic activity of V-N-codoped TiO_2 is discussed in terms of synergetic effects produced by enhanced visible light absorption and better charge separation.

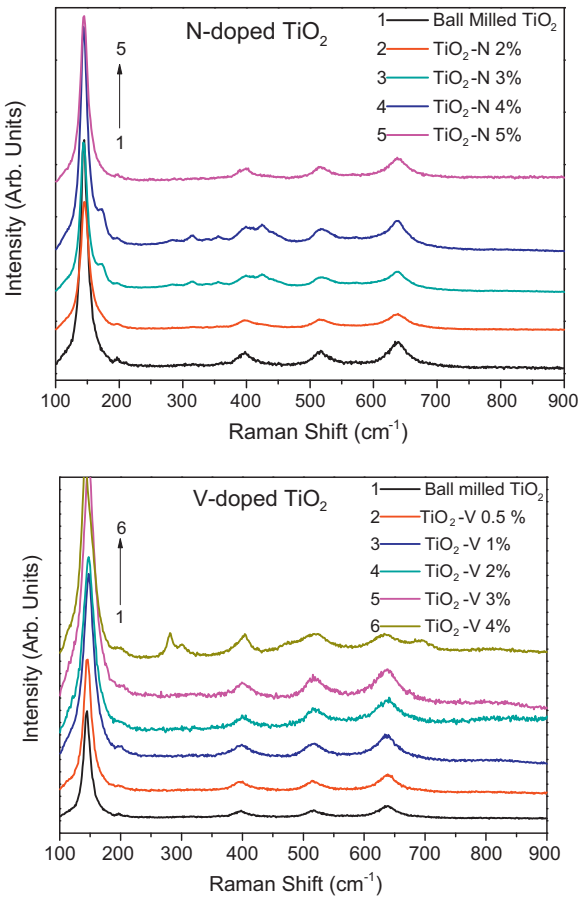

Fig. 1. Raman spectra of undoped, V-doped, and N-doped TiO_2 powders.

2. Experimental methods

Pure TiO_2 and doped TiO_2 powders were synthesized by sol–gel method using titanium butoxide [$Ti(OC_4H_9)_4$] as the precursor and nitric acid (HNO_3) as the catalyst. The molar ratio of $Ti(OC_4H_9)_4/H_2O$/ethanol/HNO_3 was kept at about 1/30/20/0.1. Undoped TiO_2 sol was prepared by first stirring the $Ti(OC_4H_6)$ and ethanol for 1 h followed by dropwise addition of water and HNO_3 mixture. The solution was stirred at room temperature for 1 h. Triethylamine [$N(CH_2CH_3)_3$] and ammonia metavanadate (NH_4VO_3) were used as sources of N and V dopants in TiO_2, respectively. During N doping, triethylamine was mixed with $Ti(OC_4H_6)$ and ethanol before addition of water and acid solution. On the contrary, for V doping the sodium metavanadate was dissolved in water and then added to the titanium butoxide solution. Different molar ratio of N source to Ti precursor (N/Ti = 2, 3, 4 and 5%) and V source to Ti precursor (V/Ti = 0.5, 1, 2, 3 and 4%) was used. V- and N-codoped TiO_2 was produced by adding $NH_4VO_3 + H_2O + HNO_3$ mixture to $[N(CH_2CH_3)_3] + Ti(OC_4H_6)$ + ethanol solution and stirred vigorously. The resulting solution was kept overnight for the gelation. TiO_2 gel was later washed 3 times with ethanol followed by drying at 125 °C for 2 h to remove the excess solvent. Later, all the resulting powders were calcinated at 450 °C for 2 h in air. All the TiO_2 powders (undoped and doped) were further ball milled at 500 rpm for 6 h for nanostructuring. After every 1 h of ball milling the samples were allowed to cool for 1 h before starting the next cycle of milling.

The surface morphology of all the samples was studied by Scanning Electron Microscope (SEM-FEG, JSM 7001F, JEOL) equipped with Energy-Dispersive Spectroscopy analysis (EDS, INCA PentaFET-x3) to determine the composition of the samples. The structural characterization of the deposited samples was carried out by detecting the mode of vibration in Raman spectroscopy. Raman spectra were recorded by using Renishaw micro-Raman spectrometer (RE-04) equipped with solid state laser with the diode pumped at 514 nm. The band gap of the doped TiO_2 was determined by measuring the UV–vis absorption spectra (taken in diffuse reflectance mode), using Cary 500 UV–vis–NIR spectrophotometer, in the range of 200–800 nm. The size of codoped TiO_2 photocatalyst nanoparticles was determined using a Transmission Electron Microscope (TEM, JEOL-JEM 2100F and energy: 200 keV). X-ray photoelectron spectra were acquired using a SCIENTA ESCA200 instrument equipped with a monochromatic Al Kα (1486.6 eV) X-ray source and a hemispherical analyzer. No electrical charge compensation was necessary to perform the analysis.

The photodegradation of rhodamine B (RhB) dye was used to evaluate the photocatalytic activities of the doped TiO_2 catalyst. 150 W xenon lamp, having closest spectral match to the solar spectrum, was used as a light source. For a photocatalytic experiment, 1 mg of photocatalyst was ultrasonically added into 3.5 ml aqueous solution of 0.2 mM RhB in a quartz beaker. The distance between the beaker and the light source was kept about 15 cm. The photocatalytic activity was determined by measuring the normalized intensity of the absorption band of RhB at 550 nm using UV–vis–NIR spectrophotometer and plotting it as a function of time of irradiation.

3. Results and discussion

Raman spectra of pure TiO_2, V-doped, and N-doped TiO_2 are shown in Fig. 1. All samples exhibit Raman peaks centered at 144, 197, 399, 513, and 639 cm^{-1} attributed to the E_g, E_g, B_{1g}, A_{1g}, and B_{2g} modes, respectively, of the anatase phase of TiO_2 [23]. This result

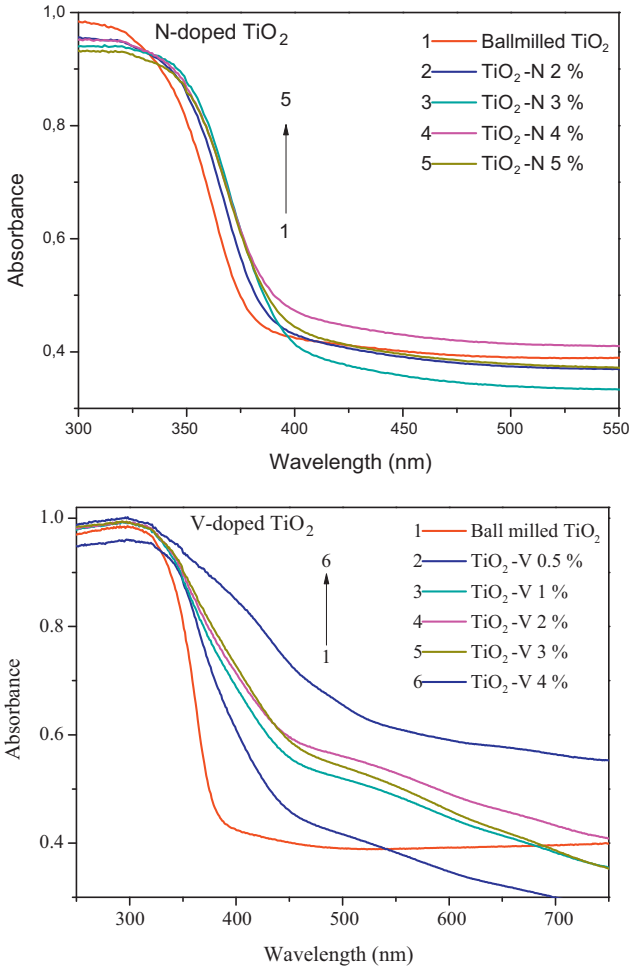

Fig. 2. UV–vis absorption spectra (taken in diffuse reflectance mode), of undoped, V-doped, and N-doped TiO_2 powders.

clearly indicates that the anatase crystal structure of the TiO_2 is well maintained even after anion (N^-) and cation (V^{5+}/V^{4+}) doping (it is well known that Raman spectroscopy can detect even minor amount of Rutile or Brokite phase). However, highest concentration of V doping (V/Ti = 4%) produces additional Raman peaks at 283, 303, 487, and 706 cm^{-1} corresponding to V_2O_5 phase [24].

The optical absorption properties of V-doped and N-doped TiO_2 were studied by measuring the UV–vis absorption spectra (taken in diffuse reflectance mode) in the range of 200–800 nm and are shown in Fig. 2. It is clearly visible from the spectra that the tail of absorption edge gets significantly shifted to the visible region for the samples with the increasing V concentration in TiO_2 powder. While in the case of N-doped TiO_2, the absorption edge gets only slightly shifted to the visible region. The band gap value is obtained by fitting the absorption edge of UV–visible spectra, using the following equation [25]:

$$\ln\ T = \ln T_0 - C\frac{(\hbar\omega - E_g)^{\nu}}{\hbar\omega} \quad (1)$$

where E_g is the band gap, C is a constant, and T_0 is the optical transmission of the substrate. Depending on the type of transition, ν assumes different values: for direct, allowed (forbidden) transitions $\nu = 1/2$ ($\nu = 3/2$) and for indirect, allowed (forbidden) transitions $\nu = 2$ ($\nu = 3$). We have used $\nu = 2$ for the present nanocrystalline or amorphous films as per the ref. [26]. Near the absorption edge, T_0 and C are approximately constant and the E_g value of all the TiO_2 samples is obtained (see Table 1) by fitting the absorption edge with Eq. (1).

Table 1
Band gap values of undoped, V-doped, N-doped and V-N-codoped TiO_2 obtained by fitting the absorption edge by Eq. (1). R is the fitting coefficient.

Samples	Band gap (eV)	R^2
Pure TiO_2	3.17 ± 0.06	0.997
Ball milled TiO_2	3.13 ± 0.06	0.996
N-doped		
TiO_2-N 2%	2.99 ± 0.06	0.994
TiO_2-N 3%	2.97 ± 0.05	0.993
TiO_2-N 4%	2.95 ± 0.05	0.991
TiO_2-N 5%	2.95 ± 0.05	0.996
V-doped		
TiO_2-V 0.5%	2.50 ± 0.05	0.999
TiO_2-V 1%	2.44 ± 0.04	0.998
TiO_2-V 2%	2.42 ± 0.04	0.998
TiO_2-V 3%	2.40 ± 0.04	0.998
TiO_2-V 4%	1.94 ± 0.03	0.997
V-N codoped		
TiO_2-V 2%-N 4%	2.31 ± 0.04	0.998

The values of band gap of 3.17 and 3.13 eV are obtained for the as synthesized and ball milled TiO_2 which are close to the theoretical values of the anatase phase (3.2 eV), thus signalling the presence of the anatase phase. The N doping causes slight decrease in the band gap to 2.95 eV in connection to the formation of localized N 2p states just above the valence band maximum of TiO_2 due to substitutional and interstitial N species [20,27]. At higher N/Ti molar ratio (4 and 5%) the density of these N 2p states increases to overlap with O 2p states and causes upward shift of valence band (VB) top. In addition, the introduced oxygen vacancies cause charge imbalance between O^{2-} and N^{3-} ions that are also responsible for visible light absorption in N-doped TiO_2 [28]. In case of V-doped TiO_2, the tail of absorption edge is prominently shifted to ~2.4 eV for V/Ti molar ratio of 1, 2, and 3%: this can be related to the charge-transfer from the 3d orbital of V ions to the conduction band of TiO_2 by forming isolated impurity energy levels below the bottom of the TiO_2 conduction band (CB) [13,29]. This means that these impurity energy levels are beneficial for extending the absorption spectrum wavelength towards the visible light region. On the contrary, the highest V-doping (V/Ti = 4%) causes the band gap to decrease to ~1.94 eV, a result mainly attributed to the presence of crystalline V_2O_5 species, having a band gap of 2 eV, on the surface of the TiO_2: this is confirmed by the Raman spectrum for the sample with 4% V doped in TiO_2 as seen in the topmost curve of Fig. 1(b).

Photocatalytic activity of V-doped and N-doped TiO_2 was tested by degradation of RhB dye. The absorption spectrum of RhB produces characteristic peak at 550 nm. Thus, by measuring the relative absorption intensity of this RhB peak, the degradation of dye, before and after the addition of TiO_2 photocatalyst, can be studied. The decolorization of dye was observed only when both TiO_2 and light irradiation are simultaneously present. The photocatalytic activity of V-doped and N-doped TiO_2 for RhB degradation as a function of time of irradiation is presented in Fig. 3.

All the TiO_2 powder samples (doped and undoped) were able, under irradiation with xenon lamp, to convert rose-red RhB solution, with initial concentration of 0.2 mM, to colorless solution (100% degradation of RhB). Irrespective of the doping concentration, the N-doped and V-doped TiO_2 showed photocatalytic activity higher than the undoped TiO_2. As the doping concentrations increase, the photocatalytic activity increases and reaches the maximum at about N/Ti and V/Ti molar ratio of 4% and 2%, for N-doped and V-doped TiO_2 respectively (inset of Fig. 3). At the highest concentrations the degradation activity of RhB decreases for the doped-TiO_2. Most significantly, V-doped TiO_2 displays considerably

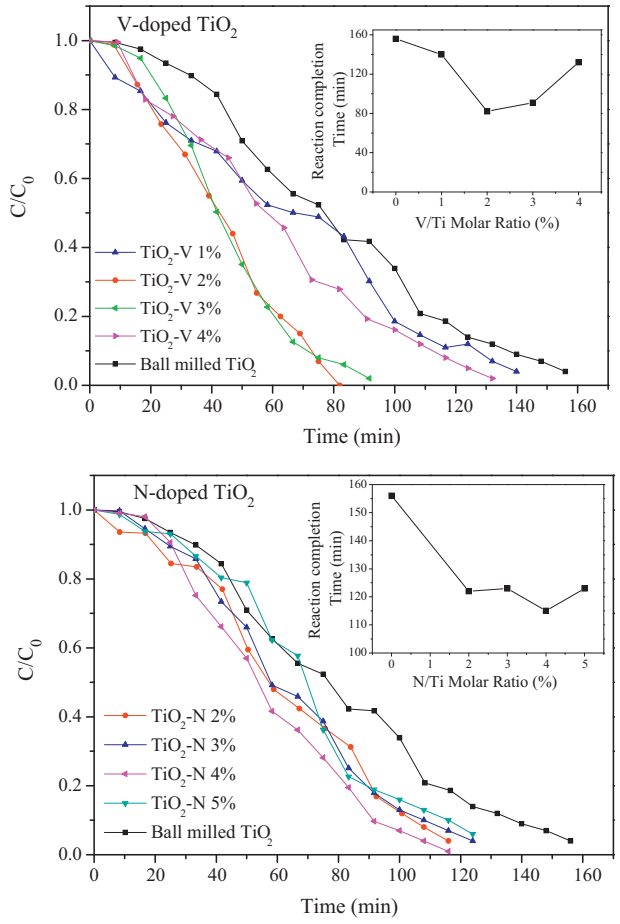

Fig. 3. Comparison of photocatalytic degradation of RhB under visible light source in presence of undoped, V-doped, and N-doped TiO_2 powders, plotted in terms of the normalized intensity of the absorption band of RhB at 550 nm in UV–vis measurements vs visible light irradiation time (lines are drawn to guide the eye). The insets show the time required for the doped-TiO_2 to produce colorless solution (100% degradation) vs molar concentration of the doped species.

better activity as compared to the N-doped samples. On the basis of these results, the molar ratio of 2% for V/Ti and 4% for N/Ti codoping was selected for further studies and henceforth this sample is designated as V2-N4-TiO_2.

The structural modification (as detected by Raman spectroscopy) and the variation in the optical absorption edge for undoped, 2%V-doped, 4%N-doped, and V2-N4-codoped TiO_2 are reported in Fig. 4 and Fig. 5 respectively. Like singly doped TiO_2, the codoped TiO_2 contains only anatase phase, as inferred from the Raman spectra (Fig. 4). As can be seen from Fig. 5, the optical absorption edge is further shifted to higher wavelength when N is added to the V-doped TiO_2. By fitting the absorption edge with Eq. (1), the band gap value of ~2.3 eV was obtained indicating that higher visible light absorption can be achieved by codoped TiO_2. Theoretical calculations performed by Ma et al. [29] using first-principles calculations in the framework of density functional theory showed that for V-N-codoped TiO_2 the hybridized states are located mainly at the edge of the VB and are composed of N 2p states while V 3d states are at the edge of the CB. Due to the strong covalent bond of V—N, the V 3d states lower the energy levels of the N 2p states to bring them closer to the VB. This enhances the mixing of N 2p and O 2p states in the VB and produces the favorable condition for trapping of holes that results in a better separation of photo-generated charges. On the contrary, the position of V 3d states are shifted to low energy regions and thus diminish any possible overlapping between V 3d and Ti 3d due to the bonding interaction between V

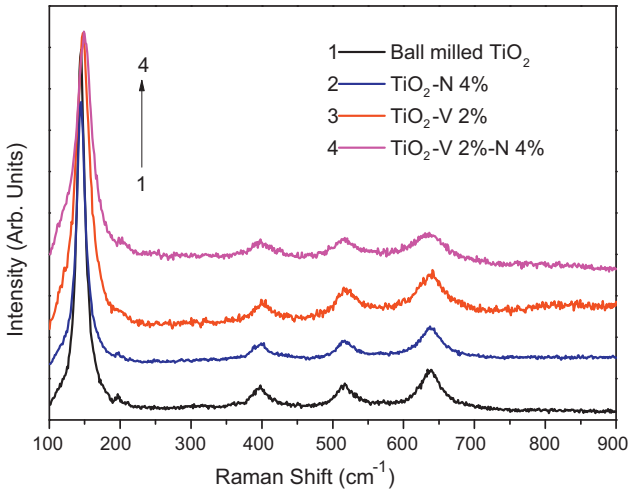

Fig. 4. Raman spectra of undoped, V2-doped, N4-doped, and V2-N4-codoped TiO_2 powders.

3d and N 2p orbitals. Thus, as compared to single element doped TiO_2, a slight variation in the position might be expected in the isolated energy levels created by V and N in TiO_2 band gap due to the interaction of V 3d and N 2p orbitals. The band gap narrowing up to 2.2 eV was calculated by Zhu et al. [30] for V-N-codoped TiO_2 using density functional theory (DFT). This value is in agreement with the present experimentally measured band gap value (2.3 eV) for V-N-codoped TiO_2.

Bright field TEM image of V2-N4-TiO_2 photocatalyst powder is presented in Fig. 6a which shows that most of the TiO_2 particles exhibit irregular spherical shapes with low level of agglomeration. The histogram of the particle size distribution measured by image processing software is presented in Fig. 6b. The particle size is distributed in narrow range of 3–14 nm with an average particle size of about ~7 nm (Fig. 6b). The standard deviation value (1.8 nm) confirms the narrow size distributions of TiO_2 nanoparticles (NPs). HRTEM image (Fig. 6c) of an individual particle clearly shows the presence of lattice fringes hence indicating the crystalline nature of the photocatalyst particle at nano-scales. The spacing between the lattice fringes was measured to be around 0.355 nm which is in good agreement with the {1 0 1} family of planes of the anatase phase (0.352 nm) [31]. SAED pattern (Fig. 6d) also shows all the distinct diffraction rings corresponding to TiO_2 anatase structure.

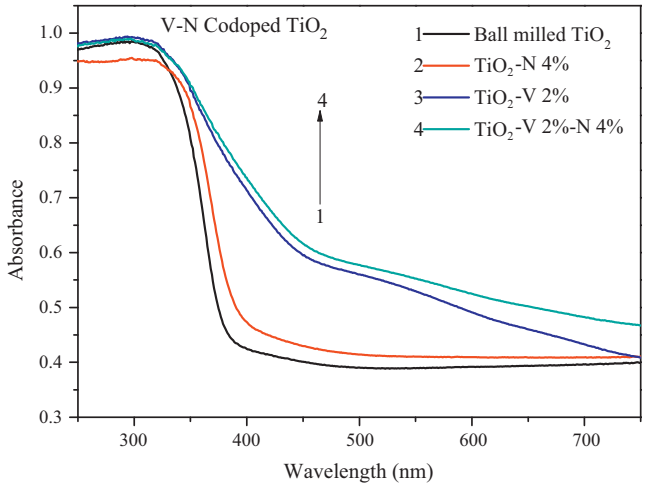

Fig. 5. UV–vis absorption spectra (taken in diffuse reflectance mode), of undoped, V2-doped, N4-doped, and V2-N4-codoped TiO_2 powders.

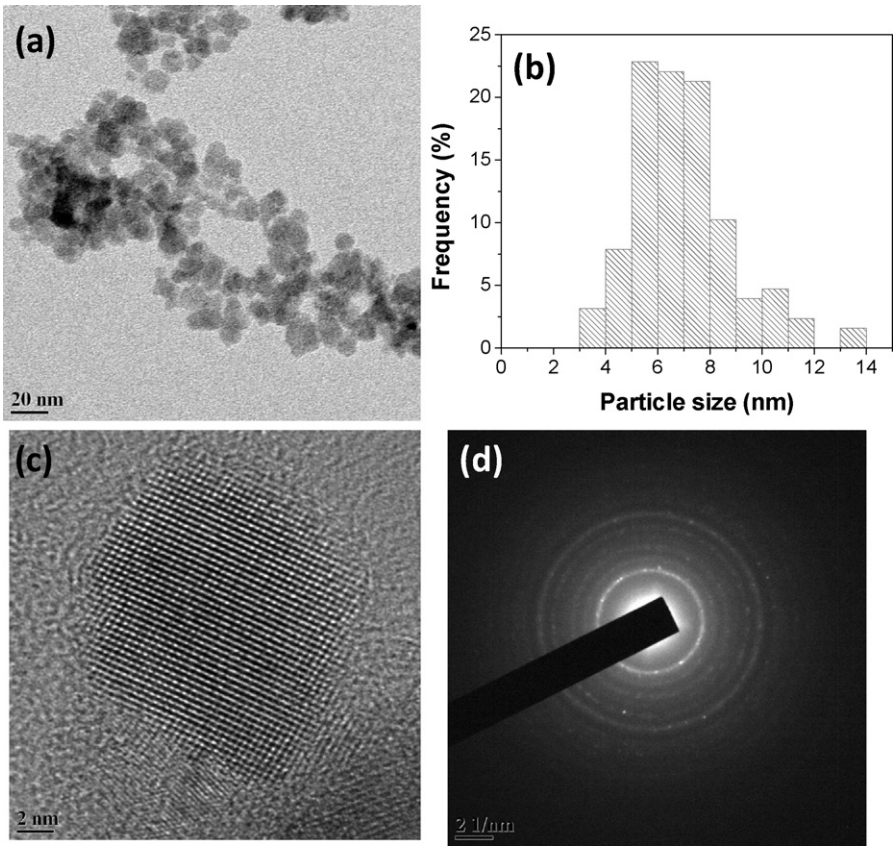

Fig. 6. (a) Bright field TEM image, (b) particle size distribution histogram, (c) HRTEM of single nanoparticle with lattice fringes, and (d) SAED pattern of V2-N4-codoped TiO_2 powder.

The chemical states of the dopants incorporated into TiO_2 were investigated by XPS. The core level of Ti2p, V2p, and N1s in V2-N4-TiO_2 photocatalyst powder is reported in Fig. 7. In Ti2p XPS spectrum, two peaks at 459.0 eV and 464.9 eV, assigned to Ti2p3/2 and Ti2p1/2, correspond to +4 valence state of Ti. Small amount (10%) of Ti^{3+} species at 457.4 eV is also observed after deconvolution of $Ti2p_{3/2}$ peak. This indicates oxygen vacancies created by the N doping. The Ti2p peak position is shifted by 0.4 eV towards positive binding energy value as compared to the standard peak (458.6 eV) [32] thus indicating that V and N ions are incorporated into TiO_2 lattice and influence the local chemical state of Ti^{4+} ions. To achieve local charge balance in the TiO_2 lattice, some of the Ti ions may acquire higher oxidation state by releasing electrons, a process that explains the XPS peak shift for V-doped TiO_2 [13]. XPS spectrum of $V2p_{3/2}$ level was deconvoluted into two peaks having binding energy values of 517.3 and 516.2 eV attributed to V^{5+} and V^{4+} states respectively [33,34]. The peak at higher binding energy (524 eV)corresponds to V^{5+}2p1/2 confriguration. This indicates that V exists in the TiO_2 in the form of V^{5+} and V^{4+}, with higher quantity of V^{5+} ions as indicated by the area under the peak in XPS spectrum. V precursor (NH_4VO_3) is the source for the V^{5+}, while V^{4+} species might have been formed during the preparation by reduction of V^{5+} species [17]. Due to similar radii, V^{4+} ions may incorporated in the TiO_2 lattice by substitutionally replacing Ti^{4+} ions and forming Ti—O—V bond [35]. In N1s XPS spectrum, a broad peak ranging from 397 to 404 eV is observed which could be deconvoluted into two peaks at 399.8 eV and 401.4 eV. There are many discrepancies in the literatures for the peak position of N-doped TiO_2. Few early reports show that the N1s peak at 396 eV is responsible for N ions that substitute oxygen ions in the TiO_2 lattice because the binding energy is close to Ti—N bond [19,36]. This peak is absent in our V-N-doped TiO_2 powder. However, several recent articles also reported the absence of 396 eV peak, instead peaks at higher binding energies at 400 eV and 402 eV are observed which are attributed to O—Ti—N linkage and Ti—N—O linkage (i.e. NO-like species), respectively [37,38]. It is possible that the N1s peak is shifted towards the higher binding energy as the presence of oxygen atom can reduce the electronic density around N atom [39]. Thus we assign the peak at 399.8 eV to N substitutionally replacing oxygen to form O—Ti—N linkage and the other peak at 401.4 eV is due to interstitial occupation of N and oxidized N species (NO) to form Ti—O—N and Ti—O—N—O linkages respectively. This result indicates that N occupies both substitutional and interstitial sites in TiO_2 lattice thus

Table 2
Photocatalytic activity of singly doped and V-N-codoped TiO_2 powders.

Photocatalyst powders	Apparent rate constant (min^{-1})	RhB degradation rate (mol/h/g of photocatalyst)
Pure TiO_2	0.007	2.94×10^{-4}
N-doped TiO_2	0.009	3.78×10^{-4}
V-doped TiO_2	0.013	5.46×10^{-4}
V-N-codoped TiO_2	0.020	8.40×10^{-4}

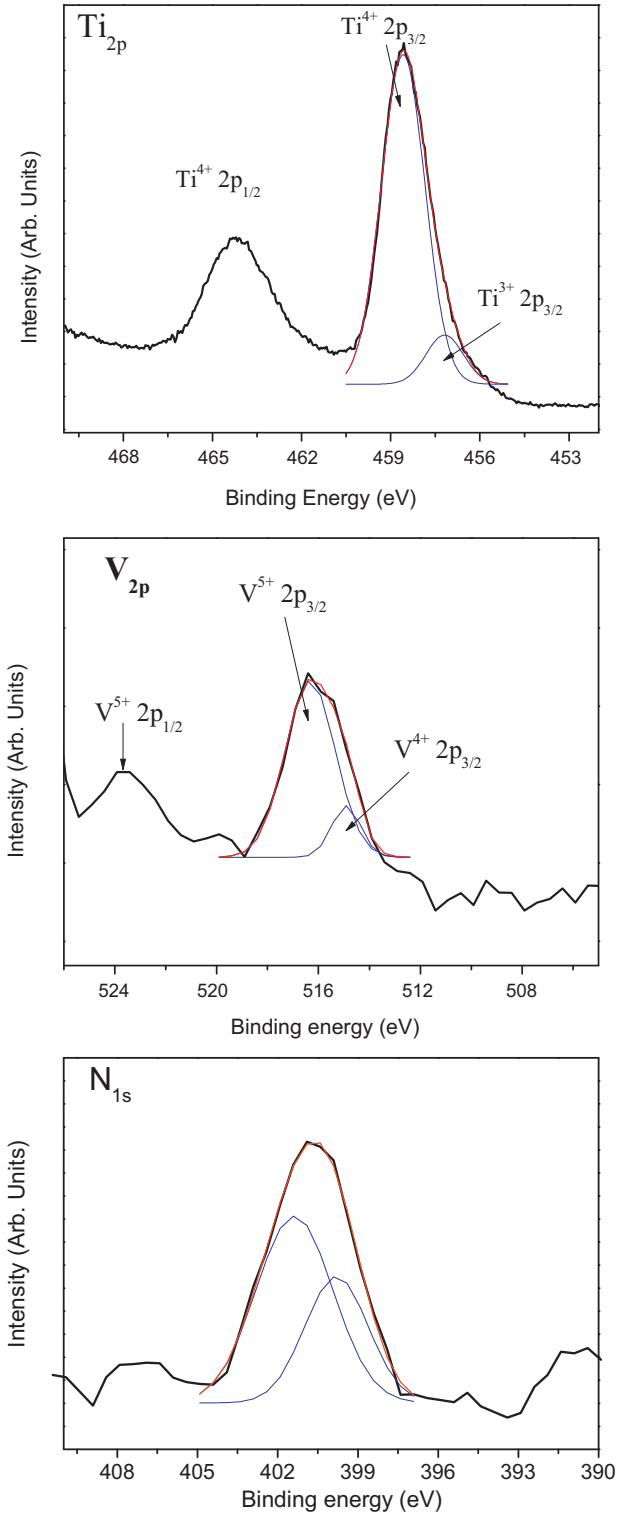

Fig. 7. XPS spectra of Ti2p, V2p and N1s levels of V2-N4-codoped TiO_2 powder.

inducing visible light sensitivity as proposed by Di Valentin et al. [40].

The photocatalytic degradation of RhB attained with V2-N4-TiO_2 is far better than both singly doped TiO_2 and undoped TiO_2 (Fig. 8). The time required for codoped-TiO_2 to produce colorless solution (100% degradation) was 2.6, 2, and 1.4 times lower than that required by pure TiO_2, N-doped TiO_2, and V-doped TiO_2, respectively. The data points in Fig. 8 were fitted linearly to

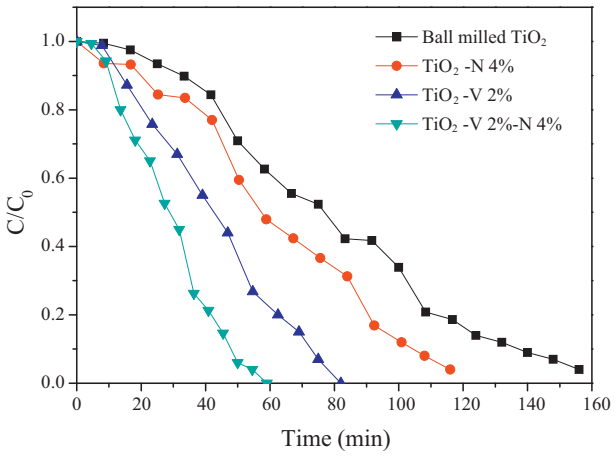

Fig. 8. Comparison of photocatalytic degradation of RhB under visible light source in presence of undoped, V2-doped, N4-doped, and V2-N4-codoped TiO_2 powders (lines are drawn to guide the eye).

calculate apparent rate constant and RhB degradation rate per gram of photocatalyst and are summarized in Table 2.

During the photocatalytic reaction, the electron and hole pairs formed in TiO_2, by the light irradiation, migrate to catalyst surface to react with absorbed O_2 and H_2O, respectively, to produce strong oxidizing agents in the form of $O_2^{\bullet-}$ and $OH^{\bullet}$ radicals, which are the main species responsible for the degradation of pollutants, RhB in our case [1]. Schematic diagram of the process is represented in Fig. 9 for photocatalytic degradation of RhB dye over V-N-codoped TiO_2 photocatalyst under light irradiation. Considering this reaction mechanism the main factors affecting the photocatalytic reaction using doped-TiO_2 are surface area, light absorption ability, charge separation, charge-carrier recombination, charge transport, doping concentration and the type of dopants. All these aspects are discussed below in details.

1. *Surface area*: Initially, the reaction takes place by absorption of O_2 and H_2O on the surface of the photocatalyst to generate oxidizing agents by electron and holes, respectively. In the present photocatalyst, the NPs with average size of ~7 nm produced by mechanical milling with good degree of dispersion provide high surface to volume ratio to increase the contact area between the active sites and the reactants, thus resulting in improved quantum efficiency of TiO_2.
2. *Light absorption ability*: In V-N-codoped TiO_2 visible light absorption efficiency is better than that of the singly doped TiO_2 (Fig. 5). As confirmed by XPS, N is incorporated in TiO_2 lattice by substitutional replacement of oxygen and by occupying interstitial site to form one or more oxidation states with oxygen (NO^-, NO^{2-}, or NO^{3-}) [39]. The substitutional N forms isolated energy

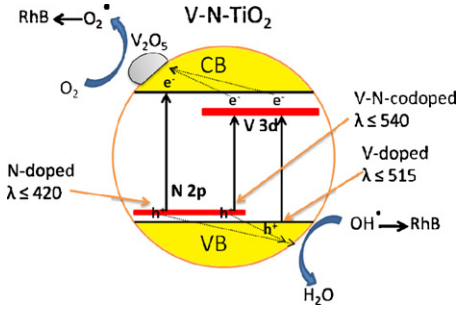

Fig. 9. Schematic diagram for photocatalytic degradation of RhB dye over V2-N4-codoped TiO_2 photocatalyst under light irradiation.

N2p level just above the VB which overlaps with O2p states at higher N concentration thus imposing slight upward shift of VB. On the contrary, the NO species formed by interstitial N has the highest energy level at about 0.73 eV above the top of the VB (Fig. 9) [39]. Moreover, N doping also creates oxygen vacancies having distinct levels in the band gap of TiO_2. On other hand, V dopants in TiO_2 are in the form of V^{5+} and V^{4+} ions: the former is from the doping precursor while later is formed by reduction of V^{5+} during calcination. This V^{4+} substitutionally replaces Ti^{4+} ions in the TiO_2 to form isolated impurity levels around 0.8 to 1.0 eV below the conduction band (Fig. 9) [13,28]. Thus these impurity energy levels created between VB and CB by V and N doping cause the absorption edge to shift further into visible region as compared to singly doped TiO_2. By improving the light absorption efficiency of TiO_2, a larger number of photogenerated charges can be formed which in turn would increase the degradation rate of pollutants: this is the case for the doped and codoped TiO_2.

3. *Type and concentration of dopant*: In V-doped TiO_2 the band gap is decreased to 2.4 eV due to the formation of V2p states in the band structure thus giving rise to higher activity as compared to N-doped TiO_2 where the absorption edge is marginally red shifted (2.95 eV) with respect to pure TiO_2 (3.2 eV). This shows that transition metal (V ions) dopant is more efficient for photocatalytic reaction than the anions dopant in TiO_2.

However, the activity increases with doping concentration, it reaches maximum for molar ratio of V/Ti = 2% and N/Ti = 4% for V-doped and N-doped TiO_2, respectively, and then decreases at higher concentration indicating an optimal concentration of dopant. The concentration of metal-dopant ions plays a very important role in photocatalytic activity. Ideally, metal ions, at low concentration, act as trapping centers for photo-generated electron (e^-) and/or hole (h^+) within the titania band gap thus increasing the recombination time of e^-/h^+ pairs.

$$\text{Electron trap}: \quad M^{n+} + e_{cb}{}^- \rightarrow M^{(n-1)+} \tag{2}$$

$$\text{Hole trap}: \quad M^{n+} + h_{vb}{}^+ \rightarrow M^{(n+1)+} \tag{3}$$

These initially trapped charges may then migrate, before recombination, towards the surface of the semiconductor where further redox reaction occurs, thus increasing the photocatalytic activity. However, a high concentration of metal ions leads to the recombination of the photo-generated e^- and h^+ as per the following mechanisms:

$$\text{Recombination center}: \quad M^{(n-1)+} + h_{vb}{}^+ \rightarrow M^{n+} \tag{4}$$

$$M^{(n+1)+} + e_{cb}{}^- \rightarrow M^{n+} \tag{5}$$

There exists an optimum concentration value of metal-dopant ions at which the maximum amount of e^- and/or h^+ are trapped without recombination; above this amount the photocatalytic activity decreases because of the increasing recombination rate.

4. *Separation, recombination, and transport of photogenerated charge carriers*: In the case of low concentration V-doped TiO_2, V^{4+} ions present in the substitutional site of Ti^{4+} in TiO_2 lattice are responsible for increased visible light absorption while V^{5+} ions present on the surface of TiO_2 particles in the form of V_2O_5 species are responsible for e^- and h^+ separation. Due to the lower Fermi level of V_2O_5 species, the photogenerated electrons may immediately transfer to V^{5+} ions leaving back holes on the TiO_2 resulting in the effective separation of e^- and h^+ [41]. The V^{4+} species, created from V^{5+} by electron trapping, easily release and transfer the electron to oxygen molecule absorbed on the surface of TiO_2 to produce superoxide radicals $O_2^{\bullet -}$ (Fig. 9). The holes in the VB react with H_2O to produce hydroxyl radicals that are indeed strong oxidizing agents required for the degradation of the dye. Similarly in N doping, due to the charge imbalance between oxygen and nitrogen ions, the N species act as the hole trapping sites to decrease the recombination process [15]. However, these dopants should be incorporated in an optimum concentration into TiO_2 because above this amount the same trapping sites act as the recombination centers. These are the reasons behind the decrease in the photocatalytic activity at high concentrations of V and N doping in TiO_2. But in the case of V2-N4-TiO_2, low V and N content helps to efficiently separate the photogenerated charges by acting as trapping sites for the electrons and holes, respectively. Thus, the probability of photogenerated charges to reach the catalyst surface before recombination is far better for codoped-TiO_2 than singly doped TiO_2.

Fast charge transfer of photogenerated charges before the lifetime is the necessary condition to achieve efficient photocatalytic activity. In the present case, the photocatalyst nanoparticles with very small size (~7 nm) and good dispersion facilitate the e^- and h^+ transport to the surface for faster reaction [30]. In addition, the presence of V^{5+} ions in the form of V_2O_5 (semiconductor with band gap of 2 eV) produces a space charge layer at the interface with TiO_2 due to difference in electrochemical potential [42]. The stationary electric field at the interface provides the driving force to the photogenerated e^- on TiO_2 to be instantaneously injected into the V^{5+} species [13]. Thus nanoparticles with V^{5+} ions provide the ideal scenario for the fast charge transfer on the surface for photocatalytic reaction. However, at higher molar ratio of V/Ti = 4 the large amount of V_2O_5 is accumulated on the surface of TiO_2, as observed in Raman spectra (Fig. 1b), to block the TiO_2 active sites for photocatalyst reaction thus resulting in decreased catalytic activity.

Considering the above discussion it may be deduced that V-N-codoped TiO_2 shows higher photocatalytic activity for the degradation of dye as compared to the singly doped TiO_2 mainly due to the synergistic effects caused by V and N that increase the visible light absorption and simultaneously act as e^- and h^+ trapping sites. The two combined effects provide ideal conditions for the charges to be photogenerated, separated, and transferred to the surface for generation of oxidizing agent.

4. Conclusions

The photocatalytic activity of V-and N-codoped TiO_2, synthesized by sol gel method, in the degradation of RhB under visible light irradiation is significantly better as compared to the undoped, V-doped, and N-doped TiO_2. The photocatalytic activity of V- and N- singly doped TiO_2 was studied to establish the optimum dopant concentration for each element. On the basis of these results, the molar ratio of 2% for V/Ti and 4% for N/Ti was selected to study RhB degradation with V- and N-codoped TiO_2. In addition, in order to increase the active surface area, the crystalline powder was ball milled to obtain nanosized particles (7 nm). The time required for codoped-TiO_2 to produce 100% degradation of RhB was 2.6, 2, and 1.4 times lower than that required by pure TiO_2, N-doped TiO_2, and V-doped TiO_2, respectively. The increased photocatalytic activity of the codoped-TiO_2 samples can be understood on the basis of two synergistic effects caused by V and N that increase the visible light absorption and at same time act as electron and hole trapping sites thus decreasing the rate of charge recombination. In particular, the V_2O_5 species, on the surface of TiO_2, having lower Fermi level with respect to TiO_2 contribute in removing the photogenerated electrons leaving back holes on the TiO_2.

Acknowledgements

We thank Raju Edla for TEM analysis, Abhijeet Bhogale for UV–vis analysis, and Lucia Calliari for XPS analysis. The research activity is partially supported by the PAT (Provincia Autonoma di Trento) project ENAM.

References

[1] U.G. Akpan, B.H. Hameed, Journal of Hazardous Materials 170 (2009) 520–529.
[2] I.K. Konstantinou, T.A. Albanis, Applied Catalysis B: Environmental 49 (2004) 1–14.
[3] W.Z. Tang, H. An, Chemosphere 31 (1995) 4158–4170.
[4] W.G. Kuo, Water Research 26 (1992) 881–886.
[5] T. Bak, J. Nowotny, M. Rekas, C.C. Sorrell, International Journal of Hydrogen Energy 27 (2002) 991–1022.
[6] A. Fujishima, X. Zhang, D.A. Tryk, Surface Science Reports 63 (2008) 515–582.
[7] M. Ni, M.K.H. Leung, D.Y.C. Leung, K. Sumathy, Renewable and Sustainable Energy Reviews 11 (2007) 401–425.
[8] W.Y. Choi, A. Termin, M.R. Hoffmann, Journal of Physical Chemistry 84 (1994) 13669–13679.
[9] M.I. Litter, J.A. Navío, Journal of Photochemistry and Photobiology A: Chemistry 98 (1996) 171–181.
[10] R. Dholam, N. Patel, A. Santini, A. Miotello, International Journal of Hydrogen Energy 35 (2010) 9581–9590.
[11] R. Dholam, N. Patel, M. Adami, A. Miotello, International Journal of Hydrogen Energy 34 (2009) 5337–5346.
[12] J. Zhu, Z. Deng, F. Chen, J. Zhang, H. Chen, M. Anpo, Applied Catalysis B: Environmental 62 (2006) 329–335.
[13] R. Dholam, N. Patel, A. Miotello, International Journal of Hydrogen Energy 36 (2011) 6519–6528.
[14] J. Ananpattarachai, P. Kajitvichyanukul, S. Seraphin, Journal of Hazardous Materials 168 (2009) 253–261.
[15] Y. Cong, J.L. Zhang, F. Chen, M. Anpo, Journal of Physical Chemistry C 111 (2007) 6976–6982.
[16] C.S. Wu Jeffrey, C. Chih-Hsien, Journal of Photochemistry and Photobiology A: Chemistry 163 (2004) 509–515.
[17] S. Klosek, D. Raftery, Journal of Physical Chemistry B 105 (2001) 2815–2819.
[18] S. Sakthivel, M. Janczarek, H. Kisch, Journal of Physical Chemistry B 108 (2004) 19384–19387.
[19] R. Asahi, T. Morikawa, T. Ohwaki, K. Aoki, Y. Taga, Science 293 (2001) 269–271.
[20] J. Liu, R. Han, Y. Zhao, H. Wang, W. Lu, T. Yu, Y. Zhang, Journal of Physical Chemistry C 115 (2011) 4507–4515.
[21] D.E. Gu, B.C. Yang, Y.D. Hu, Catalysis Communications 9 (2009) 1472–1476.
[22] J. Zhang, Y. Wu, M. Xing, S.A.K. Leghari, S. Sajjad, Energy & Environmental Science 3 (2010) 715–726.
[23] K. Yanagisawa, J. Ovenstone, Journal of Physical Chemistry B 103 (1999) 7781–7787.
[24] S.H. Lee, H.M. Cheong, M.J. Seong, P. Liu, C.E. Tracy, A. Mascarenhas, J.R. Pitts, S.K. Deb, Solid State Ionics 165 (2003) 111–116.
[25] W. Lohstroh, R.J. Westerwaal, V. Mechelen, J.L.M.C. Chacon, E. Johansson, B. Dam, R. Griessen, Physical Review B 70 (2004) 165411–165511.
[26] E.A. Davis, N.F. Mott, Philosophical Magazine 22 (1970) 903–922.
[27] D.G. Huang, S.J. Liao, W.B. Zhou, S.Q. Quan, L. Liu, Z.J. He, J.B. Wan, Journal of Physics and Chemistry of Solids 70 (2009) 853–859.
[28] Y. Nakano, T. Morikawa, T. Ohwaki, Y. Taga, Applied Physics Letters 86 (2005) 132104–132113.
[29] X. Ma, L. Miao, S. Bie, J. Jang, Solid State Communications 150 (2010) 689–692.
[30] W. Zhu, X. Qiu, V. Iancu, X.Q. Chen, H. Pan, W. Wang, N.M. Dimitrijevic, T. Rajh, H.M. Meyer III, M.P. Paranthaman, G.M. Stocks, H.H. Weitering, B. Gu, G. Eres, Z. Zhang, Physical Review Letters 103 (2009) 226401–226404.
[31] X. Yang, L. Xu, X. Yu, Y. Guo, Catalysis Communications 9 (2008) 1224–1229.
[32] R. Sanjines, H. Tang, H. Berger, F. Gozzo, G. Margaritondo, F. Levy, Journal of Applied Physics 75 (1994) 2945–2951.
[33] B.M. Reddy, P.M. Sreekanth, E.P. Reddy, Journal of Physical Chemistry B 106 (2002) 5695–5700.
[34] X. Yang, F.Y. Ma, K.X. Li, Y.N. Guo, J.L. Hu, M.X.W. Huo, H.J. Guo, Journal of Hazardous Materials 175 (2010) 429–438.
[35] J.C.S. Wu, C.H. Chen, Journal of Photochemistry and Photobiology A: Chemistry 163 (2004) 509–515.
[36] L.Z. Li, H.J. Huang, X. Chen, Z.X. Chen, W.J. Li, D. Ye, X.Z. Fu, Solid State Chemistry 180 (2007) 2630–2634.
[37] X.F. Chen, X.C. Wang, Y.D. Hou, J.H. Huang, L. Wu, X.Z. Fu, Journal of Catalysis 255 (2008) 59–67.
[38] T. Horikawa, M. Katoh, T. Tomida, Microporous and Mesoporous Materials 110 (2008) 397–404.
[39] H. Liu, G. Liu, X. Shi, Colloids and Surfaces A: Physicochemical and Engineering Aspects 363 (2010) 35–40.
[40] C.Di. Valentin, G. Pacchioni, A. Selloni, S. Livraghi, E. Giamello, Journal of Physical Chemistry B 109 (2005) 11414–11419.
[41] Y. Wang, Y.R. Su, L. Qiao, L.X. Liu, Q. Su, C.Q. Zhu, X.Q. Liu, Nanotechnology 22 (2011) 225702–225709.
[42] S. Liu, T. Xie, Z. Chan, J. Wu, Applied Surface Science 255 (2009) 8587–8592.